Chapter

Safe and Sustainable by Design Electrolytic Ni Nanocomposite Coatings: An Eco-Conscious Alternative to Hard Chromium

Alexandros Zoikis Karathanasis, Kata Berkesi, Angeliki Nikolaou, Alexios Grigoropoulos and Ioanna Deligkiozi

Abstract

Hard chromium (HC) coatings are widely used in the metal finishing industry due to their excellent wear and corrosion resistance. However, their production involves hexavalent chromium ions, a substance classified by the European Commission as toxic, carcinogenic, and mutagenic. Moreover, boric acid, which is widely used in nickel (Ni) electroplating, has been recently restricted under REACH regulations. In response, this chapter explores the development of boric acid-free Ni-based nanocomposite coatings as safer, sustainable alternatives to HC. Environment-friendly electrolytes were developed by replacing boric acid in traditional Watts-type Ni baths with safer organic acids. Candidate acids were screened, and optimized formulations were developed incorporating ceramic (e.g., SiC) and two-dimensional (2D) nanomaterials (e.g., graphene, WS_2) as reinforcing agents. Dispersion stability was ensured via the application of ultrasonication (U/S) and validated by dynamic light scattering (DLS). The Ni composite coatings were electrodeposited using both direct current (DC) and pulse current (PC) regimes under varied conditions. The structural, morphological, and mechanical properties of the coatings were evaluated using scanning electron microscopy with energy-dispersive X-ray spectroscopy (SEM-EDS), X-ray diffraction (XRD), Vickers microhardness testing, and water contact angle measurements. Corrosion resistance was assessed via Tafel polarization and electrochemical impedance spectroscopy (EIS). Results revealed that Ni/SiC and Ni/WS_2 composite coatings exhibit excellent mechanical and corrosion-resistant properties, surpassing 1,100 HV in microhardness and achieving a CR below 14.5 μm/year under certain plating conditions. A real-life example of Ni/SiC coatings in forged piston rods used in the automotive industry demonstrated strong potential for a viable and eco-friendly replacement of HC coatings.

Keywords: electroplating, boric acid-free electrolytes, reach compliant, mechanical properties, structure, pistonrods

1. Introduction to the importance of nanocomposite coatings

Hard chromium (HC) coatings are widely used in industrial applications due to their outstanding properties, including high hardness, low friction, and excellent resistance to wear and corrosion. Traditionally, electroplating has been the primary method for producing wear-resistant chromium coatings. It combines relatively low cost with the ability to generate a hard, durable finish across various scales using comparatively simple equipment. The plating process involves the electrochemical reduction of metal ions to form a metallic layer on a substrate. However, HC production depends on chromium trioxide (CrO_3), a source of hexavalent chromium – Cr(VI), which is toxic, carcinogenic, and mutagenic. As a result, its use is tightly restricted under Annex XIV of the REACH Regulation (EC No. 1907/2006), prompting the development of safer and more sustainable alternatives. This work proposes safe and sustainable by design (SSbD) coating solutions for the replacement of HC in specific applications based on nickel (Ni) matrix nanocomposite electroplating processes. The electroplated Ni-based coatings offer a promising substitute, particularly due to their good corrosion resistance and widespread use as protective finishes [1–3]. However, pure Ni lacks the mechanical robustness required for high-stress applications. To address this limitation, the concept of reinforcing Ni coatings via the incorporation of ceramic nanoparticles (NPs), such as silicon carbide (SiC), or two-dimensional (2D) NPs, like graphene (Gr) or WS_2 into the Ni matrix has become an established strategy for enhancing hardness, wear resistance, and structural stability [4–6] Their significant advantage compared to other alternative solutions to HC is that they can be produced from the existing infrastructure of plating shops by applying low-cost modifications in the lines for the safe integration of NPs, thus keeping the investment level low.

Regarding reinforcing particles, SiC NPs are the most used due to their high hardness and chemical inertness. They have been widely studied for their applicability in the automotive industry [7]. However, challenges such as NP agglomeration, sedimentation, and uneven incorporation persist, particularly when particles are nanosized [8]. Although the use of smaller particles leads to enhanced dispersion hardening and grain refinement effects, nanosized particles tend to be incorporated at lower rates into the deposit [9]. Pulse Current (PC) electrodeposition is considered as one of the most effective techniques for fabricating composite coatings, resulting in significant embedment of reinforcing particles in coatings. By tuning the PC parameters, precise control over structure, composition, wear resistance, porosity, and overall performance can be achieved [10]. In the last decade, Gr has gained significant attention as a reinforcement in electroplated Ni coatings. With its unique two-dimensional sp^2-hybridized carbon structure, Gr exhibits exceptional mechanical strength [11]. By the addition of Gr to the matrix, significant enhancement in both the corrosion resistance and wear behavior of Ni-based composites has been enabled. Another emerging alternative for Ni-based nanocomposite coating preparation is tungsten disulfide (WS_2), which acts as a solid lubricant reinforcement. Its incorporation into Ni coatings has been shown to improve hardness, reduce the coefficient of friction, and enhance overall tribological behavior [12, 13].

Moreover, several studies have concluded that ultrasonication (U/S)-assisted plating significantly enhances various characteristics of the coating, including, but not limited to, grain refinement, improved microhardness, better corrosion

resistance, more uniform surface morphology, and lower roughness. These enhancements are attributed to effects such as U/S-induced cavitation, better dispersion of reinforcing particles, reduced agglomeration, and enhanced mass transport in the electrolyte [4, 14, 15].

Despite these advancements, the electrodeposition of Ni nanocomposites continues to predominantly utilize traditional formulations, most notably the Watts-type baths. The Watts bath incorporates boric acid as a buffering agent. Boric acid, however, is classified by ECHA as a substance of very high concern (SVHC) due to its reproductive toxicity, highlighting the need for greener alternatives. Recent work has shown that organic acids of the mono-, di-, and tricarboxylic acid groups can serve as viable substitutes. Atotech Deutschland GmbH patented this approach in 2021 [16], demonstrating that the complete replacement of boric acid with tartaric acid in Watts-type baths yielded uniform, bright, and well-leveled Ni deposits in certain pH ranges. These results have enabled the practice of more environment-friendly plating chemistries.

In this work, Ni/NPs nanocomposite coatings were plated from boric acid-free electrolytes with SiC, Gr, and WS_2 as reinforcing materials. To ensure uniform dispersion of NPs in the bath, a U/S-assisted electrodeposition setup, developed in EU-funded research projects (i.e., MOZART), was employed. The direct current (DC) regime was applied for depositing all the nanocomposite systems at different current densities, while PC plating was also utilized in the case of Ni/SiC nanocomposite coatings to further enhance coating microstructure, porosity, and NP incorporation, as proved in an earlier study [17].

The goal was to surpass the mechanical properties of HC while ensuring regulatory compliance and environmental safety.

2. Materials and methods

2.1 Lab-scale electroplating of Ni/Np nanocomposites

The Ni-based nanocomposite coatings were prepared through electrodeposition at laboratory scale using a boric acid-free Watts-type electrolyte with a total volume of 1 L. The electrolyte formulation included Ni sulfate hexahydrate ($NiSO_4 \cdot 6\,H_2O$) and Ni chloride hexahydrate ($NiCl_2 \cdot 6\,H_2O$) as the primary sources of Ni^{2+} ions. Both Ni-salts were purchased from Umicore, Belgium. To replace the conventional boric acid typically used in Watts-type baths, tartaric acid ($C_6H_6O_6$, PENTA Chemicals, Czech Republic) was introduced as an alternative buffering and stabilizing agent. Regarding the reinforcing means, β -SiC NPs with an average particle size (APS) of 150 nm, supplied by MBN, Italy, were used. The Gr nano-platelets with a lateral size of 7–8 μm and a thickness of 10 nm were purchased from AVANZARE, Spain, while the WS_2 particles with an APS of 90 nm were purchased from Alroko GmbH & Co KG, Germany. To enhance the structural integrity and surface quality of the deposits, saccharin (Acros Organics, Belgium) was added to the bath as a stress-relieving agent. Saccharin also contributed to improved uniformity and brightness of the coatings. Sodium dodecyl sulfate (SDS, Sigma-Aldrich, USA) was added to the electrolyte to facilitate the dispersion of NPs. The Ni-salts were of technical grade, while all the other reagents were of analytical grade. The complete composition of the boric acid-free Ni-plating bath is summarized in

Bath formula and process parameters	**Dosage/value**
$NiSO_4.6H_2O$/(g/L)	280
$NiCl_2.6H_2O$/(g/L)	35
$C_4H_6O_6$/(g/L)	45
(a) SiC; (b) Gr; (c) WS_2/(g/L)	(a) 10.0; (b) 0.4; (c) 0.2
SDS/(g/L)	(a) 2.5; (b) 0.8; (c) 0.4
Saccharin/(g/L)	2.0
pH	4.0 ± 0.2
Cathodic current density/(A/dm^2)	1.0, 1.5, 2.0, 5.0
Plating method	Direct or Pulse current
Pulse frequency/(Hz)	10
Magnetic stirring (rpm)	250-400
Duty cyles/(%)	20, 50, 70, 90
T/(C°)	50 ± 2

The concentrations of the reinforcing agents and the corresponding sconcentrations of the SDS surfactant are denoted as follows: (a) SiC, (b) Gr, and (c) WS_2.

Table 1.
Bath formula of Ni-tartaric/Np composite baths and process parameters for performing plating.

Table 1. Electrodepositions were carried out using a high-purity Ni plate as the soluble anode and a circular brass disc as the cathode substrate with a diameter of 4 cm. Only one side of the disc was exposed to the electrolyte, while the other side was covered with masking tape, providing a plating area of 14 cm^2. Prior to deposition, the brass substrates were subjected to a standardized surface preparation protocol, including degreasing in acetone, U/S in a bath filled with reverse osmosis (RO) water, and brief etching in 10 wt% HCl to remove oxides and surface contaminants.

For the preparation of the Ni/NP nanocomposite electrolytes, the following protocol was established. At the first stage, pre-mixing of the reinforcing particles with RO water was carried out at a volume of 400 mL. U/S was applied to the water-based dispersion using a probe-type sonotrode (Hischler, 26 kHz, 1,000 W, 100% power, t_{on} = 0.5 seconds, t_{off} = 0.5 seconds) for a duration of 0.5 hours. SDS was added to the NP-water dispersion, with ratios of 1:4 for SiC and 2:1 for the 2D particles, followed by another 0.5-hour U/S-treatment. The NP-water dispersion was then transferred to the freshly prepared boric-acid-free solution of Ni-salts, and a final volume was set to 1 L. The final concentration of reinforcing particles in the electrolyte was set at 10 g/L for SiC, 0.4 g/L for Gr, and 0.2 g/L for WS_2. The U/S-sonotrode was once again applied to the nanocomposite electrolyte for 0.5 hours prior to electroplating. The dispersion characteristics of the reinforcing NPs within the electrolytic bath were evaluated using the DLS technique, conducted with a Litesizer™ 500 from Anton Paar in accordance with ASTM E3247-20. Since a high ionic strength was found in the developed Ni-bath solution and the powder loading was excessive for DLS measurements, a dilution to 0.6%–1.0% was required to ensure adequate light transmission.

The lab-scale electroplating experiments were carried out in a volume of 1 L. Ni/SiC nanocomposite coatings were produced by applying both DC and PC methods at current densities of j = 1.0, 1.5, and 2.0 A/dm^2. DC plating was performed with a RIDEN RD6012P rectifier, while the PC regime was applied using a Metrohm Autolab PGSTAT12 Potentiostat/Galvanostat system at duty cycles (d.c.) varied between 20% and 90% with a fixed frequency of 10 Hz. For the electrodeposition of the Ni/Gr and Ni/WS_2 nanocomposite coating systems, experiments were conducted applying only the DC plating regime with a current density range of j = 5.0 A/dm^2 as indicated by previous studies incorporating 2D particles in Ni coatings [18].

During electrodeposition, constant magnetic stirring was employed to maintain uniform hydrodynamics and stable particle dispersion. The bath temperature was maintained at 50°C ± 2°C, and the pH was adjusted within the range of 3.8–4.2 using an aqueous ammonia solution. Deposition time was regulated to achieve a theoretical coating thickness of approximately 30 μm, based on Faraday's Law [19]. The crystallographic structure of the coatings was analyzed using a PROTO AXRD Benchtop X-Ray Diffractometer (PROTO Manufacturing, Canada). The measurements were performed using Cu Kα radiation (λ = 1.5406 Å) generated at an operating voltage of 30 kV and a current of 20 mA. All diffraction data were processed, and peak positions were refined using standard procedures compliant with ISO 22278:2020. The average crystallite size of the Ni was calculated using the Debye-Scherrer method [20]. The scanning electron microscopy with energy-dispersive X-ray spectroscopy (SEM-EDS) measurements were conducted using a Tescan Vega Compact microscope (Tescan, Brno, Czech Republic), equipped with an EDAX EDS detector. The SEM image magnification and beam parameters were calibrated in accordance with ISO 16700:2016. Quantitative elemental analysis by EDS followed the recommendations of ASTM E1508-12a(2022). For selected samples, the coating thickness was verified on cross-sectional images according to ISO 9220:2022. The wettability of the surfaces of the Ni/2D coatings was probed through water CA measurements using a Biolin Scientific optical tensiometer. RO-water was used as the probe liquid. Each contact angle (CA) was determined via the sessile drop method, with the droplet contour fitted by the Young–Laplace equation. The testing and data evaluation procedure was performed as outlined in ASTM D7334-08(2020). All measurements were performed under ambient laboratory conditions. The Vickers microhardness was determined using a Shimadzu HMV-G20 Micro Hardness Tester, allowing for precise and accurate assessments of the coatings' hardness. The procedure followed the specifications of ISO 6507–1:2018. The surface preparation and indentation spacing were selected according to ASTM E384-17, ensuring reproducibility and avoiding the influence of adjacent impressions. Reported hardness values represent the mean of at least 10 valid indentations per sample.

To evaluate the corrosion properties of the nanocomposite coating, the Tafel polarization method and EIS [21] were applied via a VersaStat 3 Potentiostat by Princeton Applied Research, controlled by VersaStudio software. The corrosion measurements were performed in a three-electrode flat-bottom cell from Metrohm AG, Switzerland. The coated sample was placed at the bottom of the cell as the working electrode with an exposed area of 4.6 cm^2. An Ag/AgCl (in 3 M KCl) electrode was used as the reference electrode. A circular-shaped stainless-steel electrode positioned above the coating was applied as the counter electrode. A 3.5% NaCl solution was used as the corrosive medium. Potential values were automatically

corrected by VersaStudio during the measurements and are demonstrated versus the standard hydrogen electrode (SHE). Tafel polarization measurements followed the procedure described in ISO 17475:2005. The polarization curves were recorded after stabilization of the open-circuit potential (OCP) for approximately 30 minutes following the immersion of the working electrode in the corrosive medium. The measurements were performed within a potential range of –0.6 V to + 0.4 V relative to the OCP, at a scan rate of 3 mV/s. The corrosion potential (E_{corr}) and corrosion current density (I_{corr}) were determined from the extrapolation of the anodic and cathodic branches. The EIS measurements were carried out as described in ISO 16773–2:2016, ensuring reliable data collection and interpretation for coated metallic substrates. In practice, after the Tafel test, an additional 10-minute OCP stabilization was applied in the same cell setup, followed by impedance measurements in the frequency range of 10^5–10^{-2} Hz with an amplitude of 10 mV (rms) around the DC potential of 0.025 V versus OCP.

2.2 Pilot-scale electroplating of Ni/SiC nanocomposites

The Ni/SiC system was selected for the pilot-scale validation of the developed Ni-tartaric-based electrolyte. The pilot-scale electroplating of Ni/SiC nanocomposite coatings was carried out on forged steel piston rods (DIAD Group, Italy), 30 cm in length and 0.8 cm in diameter. The rods were plated with the developed SSbD Ni/SiC coating and were fully characterized to provide insight into the coating properties. The composition of the bath was identical to the composition shown in **Table 1**. The deposition process was conducted using an electroplating pilot line of 250 L volume, divided into two compartments: Main and Auxiliary (AUX) sub-tanks (V ~125 L each). The agitation/circulation between the sub-tanks was ensured by two high-performance diaphragm pumps (Alpha Dynamic Pumps, Greece). The temperature of the bath was maintained via an immersion heater (Mazurczak GmbH, Germany) and PLC controller. To ensure a good dispersion of the SiC NPs in the Ni-tartaric electrolyte, a custom-made U/S panel (25 kHz, 2,000 W) was applied, immersed, and fixed on the inner wall of the AUX tank.

Prior to electroplating, all piston rods were subjected to a standardized pre-treatment process of degreasing by anodic electrocleaning in NaOH, pickling in H_2SO_4 solution to eliminate surface oxides and activate the substrate, and deposition of a ~5 μm metallic Cu interlayer, plated from an acidic Cu bath with j = 5 A/dm^2. This intermediate layer was applied to improve adhesion between the steel substrates and the Ni/SiC nanocomposite coating. The copper-coated rods were activated via immersion in 10% HCl for 30 seconds and were then mounted to a custom-made rotating rack system. The rods in the rack system were continuously rotated during the plating via a motor at a speed of 12 rpm to ensure homogeneous current distribution on the surface of the rods. Prior to plating, a 30-minute U/S treatment was applied via the U/S panel in the AUX tank. DC and PC current regimes were tested, with and without the periodical imposition (15 minutes on and 15 minutes off) of U/S during electroplating, indicated as "U/S$_{on/off}$" and "U/S$_{off}$", respectively. For the PC plating, a d.c. of 50% and a pulse frequency of 10 Hz were used. The current density of j = 1.5 A/dm^2 was selected for plating. The duration of the plating was set to reach the theoretical thickness of 50 μm. Electrodeposition was performed using an AxD power supply generator (A1D 150/300 LV20 G4) from MUNK GmbH, The Netherlands.

The crystallographic, morphological, mechanical, and electrochemical corrosion properties of the coatings were investigated using X-ray diffraction (XRD), SEM-EDS, Vickers microhardness testing, Tafel, and EIS studies, respectively. XRF measurements were conducted using a portable NITON XL5 XRF tester by Thermoscientific, providing a rough elemental composition of the pilot-scale electroplated nanocomposite coatings containing SiC NPs.

3. Results and discussion

3.1 Dispersion stability of the electrolyte

The complete summary of DLS results is presented in **Table 2**. Across all Ni-tartaric/NP nanocomposite bath dispersions, the mean hydrodynamic diameter (HDD) of the suspended particles remained below 1 μm, confirming satisfactory colloidal stability prior to electrodeposition. The observed hydrodynamic diameters (HDD ≈500–600 nm) and a polydispersity index of ≈20% for the Ni/SiC system were found to be consistent with prior reports of SiC dispersions in Ni-based plating media. Rao et al. [22] measured an average HDD of 544 nm for SiC treated with surfactant. The Gr-based dispersion yielded HDD values around 1 μm, while the WS_2 particles demonstrated HDD ranging between 740 and 950 nm. A ζ-potential in the range of −20 to −30 mV was measured for all three NPs in the electrolyte. Depending on the type of NPs in the Ni–tartaric bath, moderate electrostatic stabilization was indicated.

3.2 Crystallographic evaluation of the Ni/NPs coatings

3.2.1 Lab-scale electroplated Ni/NP nanocomposite coatings

The influence of NP incorporation on the crystal structure and texture evolution of the Ni-matrix was determined through diffraction patterns. The XRD patterns of the pure Ni (black), the Ni/SiC (red), Ni/Gr (blue), and Ni/WS_2 (magenta) nanocomposite coatings plated from the Ni-tartaric acid-based bath using the DC method at j = 1.0 A/dm^2 are shown in **Figure 1**. More specifically, **Figure 1(a)** shows the XRD patterns of all coatings, in which four prominent peaks at 2θ = 44.5°, 51.85°, 76.37°, and 93.05° are observed corresponding to the (111), (200), (220), and (311) crystallographic planes of face-centered cubic (fcc) Ni, respectively. The Ni(111) reflection was identified as the dominant peak, indicating a (111)-preferred crystallographic orientation, which is commonly observed for electrodeposited Ni

Nanoparticle	HDD (nm)	PDI (%)	ζ-potential (mV)
SiC	490–570	20 ± 8	−28 ± 4
Gr	930–1,090	27 ± 4	−30 ± 3
WS_2	740–950	38 ± 6	−20 ± 2

Table 2.
Results of DLS measurements on the dispersion of NPs in the Ni-tartaric acid-based electrolyte.

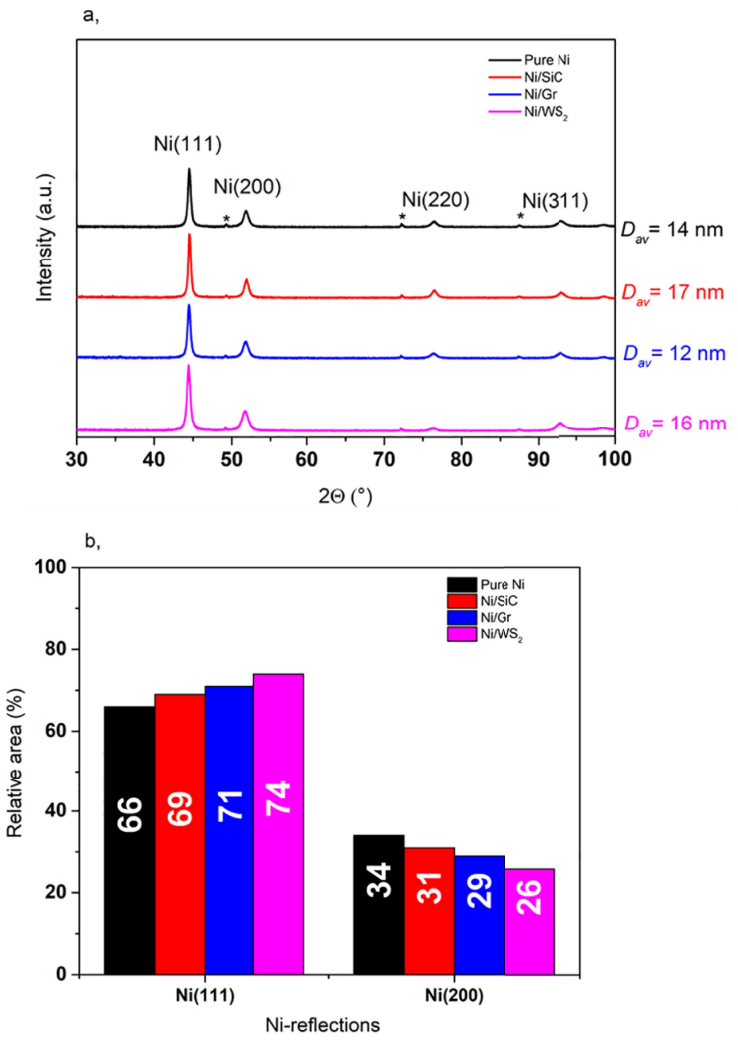

Figure 1.
*(a) XRD patterns and corresponding average crystallite sizes (D_{av}) of coatings electrodeposited from a Ni–tartaric acid-based electrolyte using DC method at j = 1.0 A/dm^2. (b) Relative intensities of the two dominant Ni crystallographic orientations. Color coding: Pure Ni (black), Ni/SiC (red), Ni/Gr (blue), and Ni/WS_2 (magenta). *Indicates peaks assigned to the brass substrate.*

and Ni-based nanocomposites [12, 23]. No secondary Ni phases were introduced by the addition of SiC, Gr, and WS_2; however, slight alterations of the relative intensities of the Ni(111) and Ni(200) reflections were observed and are depicted in **Figure 1(b)**. The average crystallite sizes (D_{av}) calculated using the Scherrer equation for the pure Ni, Ni/SiC, Ni/Gr, and Ni/WS_2 coatings were 14, 17, 12, and 16 nm, respectively. These values fall within the ranges previously reported for electrodeposited Ni composites under similar plating conditions [24].

The incorporation of SiC particles did not lead to grain refinement in the Ni-matrix. The D_{av} in the plated SiC-containing Ni coatings was slightly higher compared to pure Ni under similar electroplating conditions. However, grain refinement was promoted by the incorporation of Gr into the Ni-matrix. The growth

of reduced grains was hindered, and additional nucleation sites were simultaneously provided by the embedded Gr [24]. As for the effect of WS_2 on the calculated D_{av} in the Ni/WS_2 coating, the value of 16 nm was found to be consistent with the reported ~14 nm for Ni–Co/WS_2 composites [25].

3.2.2 Pilot-scale electroplated Ni/SiC nanocomposite coatings

The XRD patterns of Ni/SiC coatings deposited using DC and PC plating methods, both U/S_{off} and U/$S_{on/off}$ during deposition, together with the calculated average Ni crystallite size, are shown in **Figure 2(a)**. For comparative reasons, XRD patterns of the pure Ni plated with DC and PC without U/S were added to the figure. The XRD patterns displayed four prominent peaks at 2θ = 44.5°, 51.85°, 76.37°, and

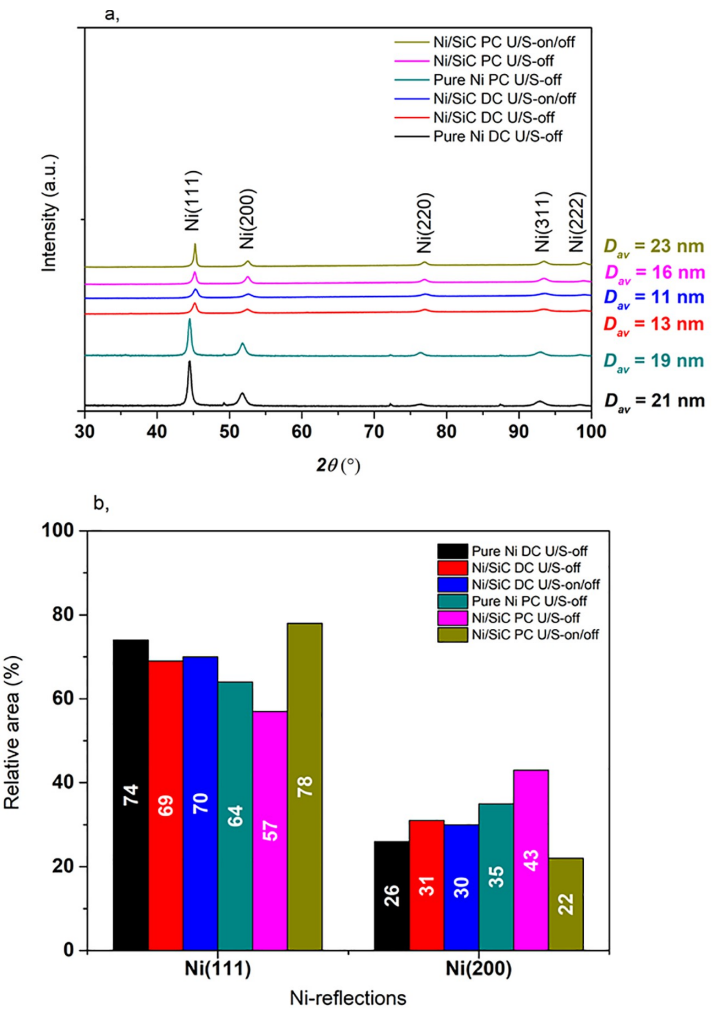

Figure 2.
(a) XRD patterns with average crystallite size (D_{av}) of Ni and (b) relative peak areas of the main Ni reflections for pure Ni plated with DC (black) and with PC (teal) U/S_{off}; and for Ni/SiC-coating deposited with DC U/S_{off} (red), DC U/$S_{on/off}$ (blue), PC U/S_{off} (magenta), and PC U/$S_{on/off}$ (dark yellow).

93.05°, which correspond to the (111), (200), (220), and (311) crystallographic planes of face-centered cubic (fcc) Ni, respectively. This led to significantly stronger diffraction intensities from the Ni phase, which may overshadow the relatively weaker signals originating from the SiC phase. The D_{av} of the pure Ni coatings (black) was determined to be 21 nm in the DC regime and U/S_{off} method, while the D_{av} of Ni/SiC coatings plated under similar conditions (red) was significantly reduced to was ~13 nm. A further decrease in Ni-grain size to 11 nm (blue) in Ni/SiC was observed when the $U/S_{on/off}$ method was employed during plating. This supports the idea that particle incorporation disturbs growth and facilitates the creation of more nucleation sites [23].

The PC-plated coatings with U/S_{off} showed a slight reduction in D_{av} for pure Ni coatings, from 21 nm in DC mode (black) to 19 nm in PC mode (teal). However, the D_{av} of Ni/SiC U/S_{off} coatings plated with PC plating did not follow this trend, as they resulted in an increase in the Ni grain size from 13 nm in DC mode (red) to 16 nm in PC mode (magenta). A further increase in D_{av} was observed, to 23 nm in PC plating mode with $U/S_{on/off}$ (dark yellow). This behavior can be attributed to the complex interactions between SiC NPs, the intermittent current flow of PC plating, and enhanced ion transport due to U/S [15]. The NPs, while promoting grain refinement under DC by acting as heterogeneous nucleation sites, may agglomerate or interfere with nucleation during off-times in PC plating, leading to coarser grains [15].

A preferred orientation toward the Ni(111) plane was observed across all samples by comparing the relative peak areas of the Ni(111) and Ni(200) reflections, as shown in **Figure 2(b)**. Pure Ni coating demonstrated a strong intrinsic preference for Ni(111) orientation, with 74% (black) under DC conditions, while PC plating reduced the Ni(111) intensity to 64% (teal) of pure Ni. The incorporation of SiC particles in the Ni matrix under DC conditions led to a moderate decrease in Ni(111) texture to 69%–70% (red and blue, respectively).

For Ni/SiC U/S_{off} coatings produced with PC plating, a significant reduction in Ni (111) texture was observed, with 57% of Ni(111) (magenta). In contrast, with $U/S_{on/off}$, Ni/SiC coatings exhibited a significant increase in the texture along the (111) plane, with the Ni(111) reflection increasing to 78% (dark yellow). Interestingly, this texture strengthening occurred despite an increase in crystallite size to 23 nm, indicating that $U/S_{on/off}$ promoted directional grain growth rather than grain refinement under these conditions. These results suggest that while SiC NPs contributed to grain refinement under DC deposition, they may inhibit effective nucleation under PC conditions due to agglomeration or particle-interface interactions [26]. The $U/S_{on/off}$ applied to the PC-plated coating significantly enhanced mass transport and reduced hydrogen bubble entrapment, thereby promoting anisotropic crystal growth and sharper texture, particularly along the Ni (111) plane. However, the same $U/S_{on/off}$ conditions may have also accelerated the growth of existing grains rather than initiating new nuclei, leading to grain coarsening in composite coatings [27].

3.3 Morphological analysis of the Ni/Np coatings

3.3.1 Lab-scale electroplated Ni/Np nanocomposite coatings

The SEM images of pure Ni and Ni/NP coatings plated from a Ni-tartaric acid-based bath under the DC plating method at $j = 1.0\ A/dm^2$ are shown in **Figure 3**.

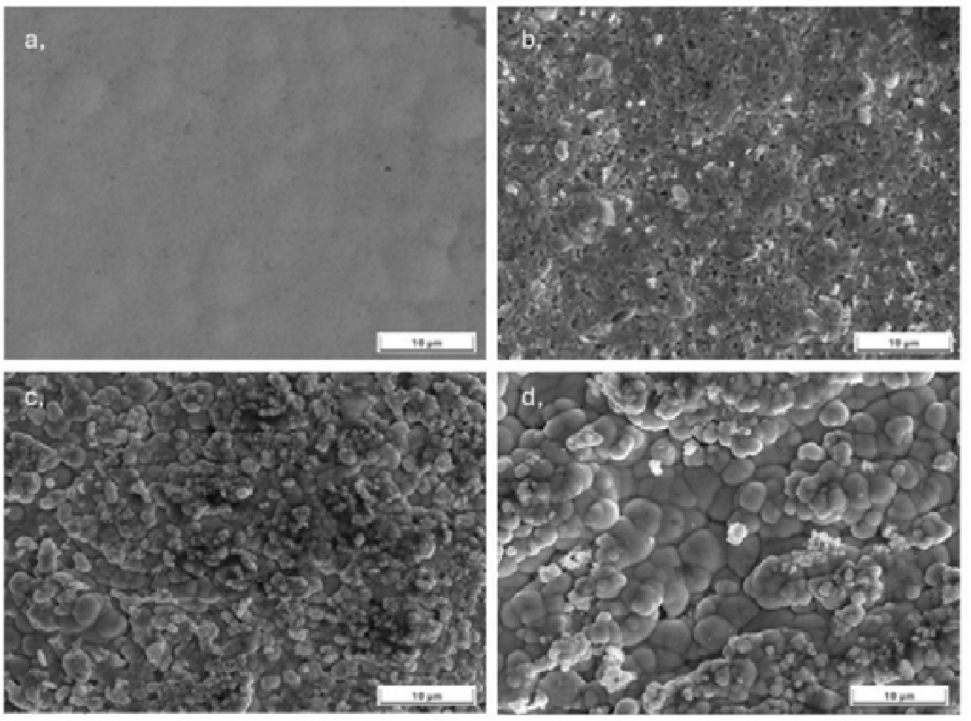

Figure 3.
(a) SEM image of (a) pure Ni and (b) Ni/SiC nanocomposite coating, (c) Ni/Gr and, (d) Ni/WS_2 plated from Ni-tartaric acid based bath with DC plating method at j = *1.0 A/dm*^{2}.

In **Figure 3(a)**, a smooth and uniform surface morphology was revealed by the SEM micrograph of the pure Ni coating, indicating that a homogeneous and well-controlled deposition was achieved. The SEM images of the Ni/SiC nanocomposite coating shown in **Figure 3(b)** reveal a uniform distribution of the embedded particles. Such homogeneous dispersion of the reinforcing particles is regarded as essential for producing a structurally consistent nanocomposite coating and is directly associated with the improvement of mechanical and functional properties across the entire surface [28]. The EDS was employed to further investigate the distribution of the respective NPs in the nanocomposite coatings. The EDS analysis revealed a Si-content of 8 ± 2 wt%. The morphology of the Ni/Gr nanocomposite coating is illustrated in the SEM image shown in **Figure 3(c)**. Distinct Gr sheets could be discerned on the surface, appearing as thin, wrinkled, veil-like structures that cover regions of the Ni matrix [29]. These sheets imparted a more open, coarse, and granular surface texture compared to the smooth morphology of pure Ni. Darker surface regions were also evident, consistent with the presence of Gr. The localized enrichment of carbon (up to 26.5 wt%), confirmed by elemental mapping via EDS, further supported the incorporation of Gr. It should be noted that, due to the limitations of EDS in accurately quantifying low-Z elements such as carbon, the carbon values were interpreted qualitatively rather than quantitatively. The SEM image shown in **Figure 3(d)**, related to the Ni/WS_2 nanocomposite coating, showed a nodular rough surface with characteristic cauliflower-like structures.

The formation of these structures was primarily attributed to the preferential adsorption and accumulation of Ni ions on the clustered WS_2 during the electrodeposition process [25]. This could be explained by the presence of WS_2 nanosheets influencing the local electric field distribution, as the initially embedded WS_2 altered the current density distribution. Localized areas of higher current density were generated around the WS_2 sites, further influencing the growth dynamics of the deposit and contributing to the observed surface morphology [24]. In addition, the presence of WS_2 nanosheets was confirmed through EDS analysis, which revealed a localized tungsten content reaching 2.5 wt%.

3.3.2 Pilot-scale electroplated Ni/SiC nanocomposite coatings

The SEM was utilized to thoroughly assess the microstructure, morphology, and surface topography of the pilot-scale electrodeposited Ni/SiC nanocomposite coatings. The Ni-to-Si weight ratio was quantitatively determined by EDS analysis.

The SEM images conducted on a Ni/SiC-coated piston rod are shown in **Figure 4**. The samples were prepared using the DC plating method for both (a) U/S_{off} and (b) $U/S_{on/off}$ methods. It was distinctly revealed in **Figure 4(a)** that U/S_{off} led to a rough, porous, and cauliflower-like surface with a nodular structure. The EDS map analysis of the area detected a Si content of 4–6 wt%. On the contrary, the SEM image shown in **Figure 4(b)** indicated that the $U/S_{on/off}$ method led to more compact, uniform nodules and resulted in grain refinement, which findings are in accordance with the study by Pinate et al. [15]. The EDS map analysis revealed that the Si content in this sample was around 7–8 wt%.

The SEM images of samples prepared with PC $U/S_{on/off}$ are shown in **Figure 5(a)** and **Figure 5(b)** at different magnifications (4k×, 10 k×). The compactness and uniformity of the coating were further enhanced by the PC plating method [30]. Additionally, a more homogeneous distribution of SiC NPs in the Ni-matrix was evident. The EDS map analysis revealed a Si-content of around 4–6 wt%.

A cross-section SEM-EDS analysis was conducted on the Ni/SiC coatings plated on piston rods (see **Figure 6**). An even distribution of SiC NPs in the Ni-matrix was identified in **Figure 6(a)**, plated using the DC and U/S_{off} method. Based on the EDS mapping analysis performed on the Ni/SiC coating, a Si-content of 9 wt% was

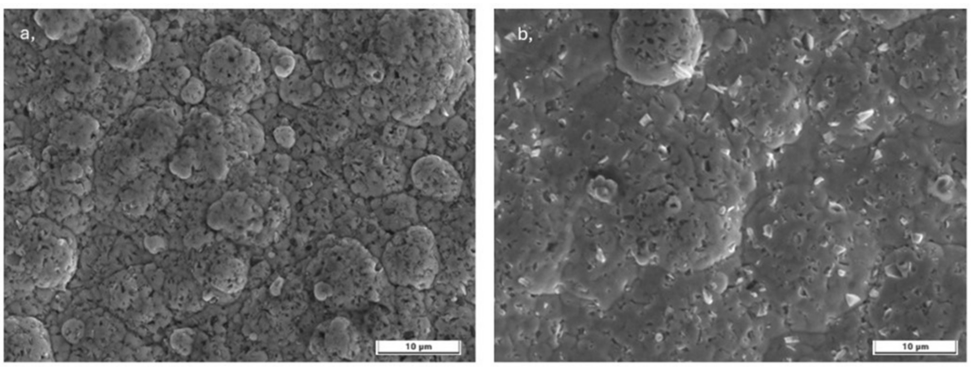

Figure 4.
SEM image of Ni/SiC coating prepared with DC plating and (a) US_{off} and (b) $US_{on/off}$.

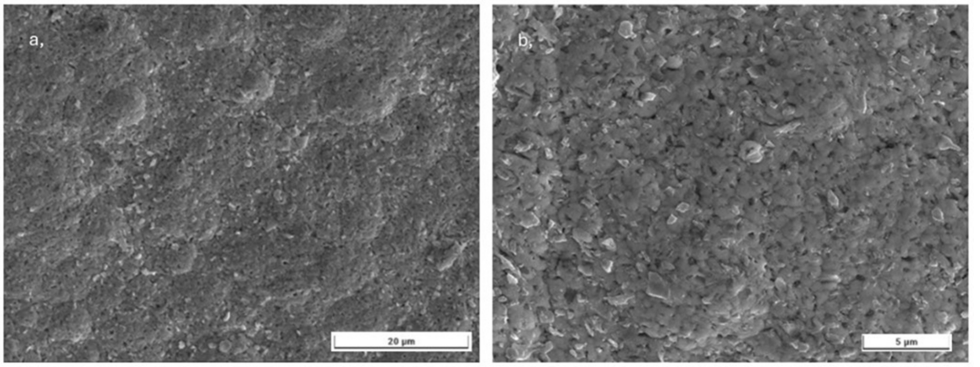

Figure 5.
SEM images at magnifications of (a) 4k×, and (b) 10k× of Ni/SiC coatings prepared using the PC plating method at j = 1.5 *A/dm*^{2} *under periodic U/S*$_{on/off}$ *conditions during plating.*

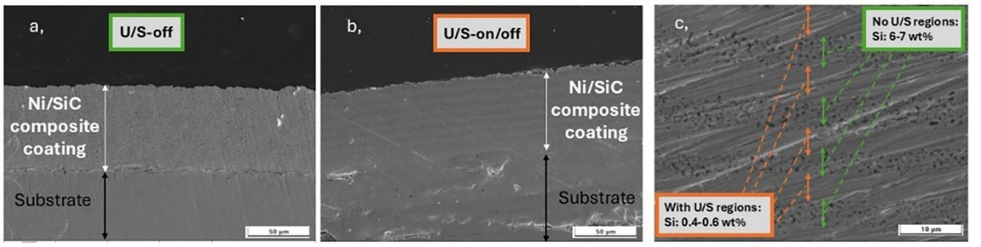

Figure 6.
Cross-sectional SEM image of a Ni/SiC coating plated on a piston rod with DC and (a) U/S$_{off}$ *(1k× magnification); and U/S*$_{on/off}$ *at (b) 1k×, and (c) 5k× magnifications. The Si-content in the U/S*$_{off}$ *layers is 6–7 wt%.*

observed. A cross-section SEM image of the DC U/S$_{on/off}$ coated sample is shown in **Figure 6(b)**. The imposition of a 15-minute long U/S$_{on}$ period, followed by a 15-minute U/S$_{off}$ cycle, significantly affected the morphology of the coating. In this case, the Ni/SiC coating exhibited distinct layers containing lower and higher amounts of Si, each approximately 7–9 µm thick. This structure is directly correlated to the periodic introduction of U/S-treatment of the dispersion during plating. During periods when U/S was turned off, a higher degree of SiC NP incorporation was evident in the SEM images, indicated by darker spots. In contrast, during the periods when U/S was turned on, the Ni matrix showed a marked reduction in SiC NP incorporation. The EDS analysis of these layers identified 0.4–0.6 wt% Si-content, as shown in the higher magnification image in **Figure 6(c)**. This observation suggests that the incorporation of SiC NPs into the coating during active U/S$_{on}$ periods was hindered by the U/S waves. On the contrary, the EDS map analysis revealed an average Si-content of around 6–7 wt% in the layers deposited with U/S$_{off}$.

The SEM images of the coating plated using PC U/S$_{on/off}$ are shown in **Figure 7**. Similar to the DC coatings, a varying SiC content was identified in the alternating layers, corresponding to the periodic use of U/S during plating. It should be mentioned that an initial thickness of 20 µm of the coating was deposited with U/S$_{off}$. This served as a further enhancement of the adhesion between the Ni/SiC

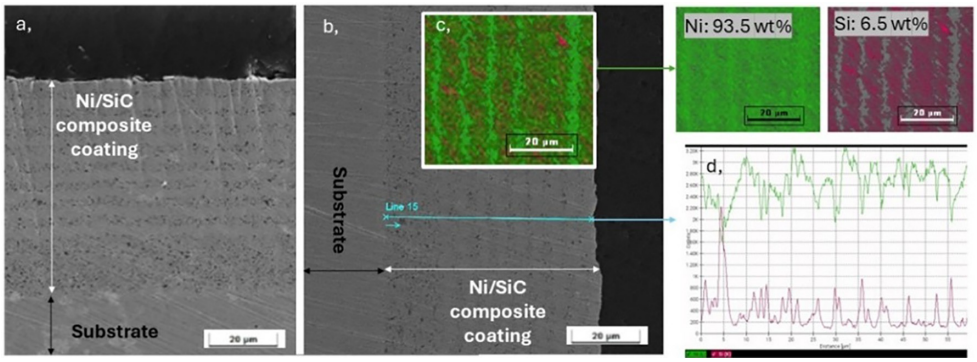

Figure 7.
Cross-sectional SEM images of Ni/SiC coating prepared under PC U/$S_{on/off}$ at (a) 2k× (b) 4k× magnifications, (c) EDS mapping analysis, and (d) EDS line analysis of the coating.

layer and the adhesive Cu-sublayer surface. It was followed by the application of U/$S_{on/off}$ for the remaining duration of the deposition. It is clearly shown that the SiC incorporation in the Ni-matrix was greatly affected by the application of U/S, with distinct SiC-rich and SiC-poor layers being observed.

According to the EDS mapping analysis shown in **Figure 7(c)**, the average Si-content in the examined area was approximately 6.5 wt%. As a result of the EDS line scan, a similar Si content, around 5.8 wt%, was identified, as depicted in **Figure 7(d)**. The influence of the presence of U/S waves on the Si-incorporation into the Ni-matrix was greatly supported by these results. A possible explanation for this structure is that SiC NPs, which are only loosely attached to the surface of the growing coating, are displaced under the influence of U/S waves. Beyond their role in dispersion stability, U/S treatments are also widely recognized for promoting surface decontamination and the removal of loosely bound particles. Thus, during the U/S_{on} period, two phenomena occur in the system. On the one hand, the dispersion of SiC in the electrolyte is enhanced, resulting in a finer distribution of NPs in the composite coating during the U/S_{off} period. On the other hand, the co-deposition rate is markedly reduced, resulting in intermediate layers with a lower SiC content.

3.4 Mechanical properties of the Ni/Np coatings

3.4.1 Lab-scale electroplated Ni/Np nanocomposite coatings

The Vickers microhardness values of the plated Ni/SiC coatings are represented in **Figure 8.** Specifically, **Figure 8(a)** compares coatings deposited from the conventional Watts-bath with those from the Ni-tartaric acid bath. Coatings produced using both DC (a.1) and PC–d.c. 50% (a.2) methods are shown. The plating was carried out at current densities of j = 1.0, 1.5, and 2.0 A/dm^2. For the Ni/SiC coatings deposited from the Ni-Watts/SiC electrolyte, hardness values ranged from 292 ± 24 HV to 428 ± 24 HV (black columns), which are consistent with literature reports [10, 22]**.** A significant increase in microhardness was observed when boric acid was replaced by tartaric acid in the Ni-bath. The highest average hardness of 1,011 ± 223 HV was measured on coatings deposited at j = 1.5 A/dm^2 under DC

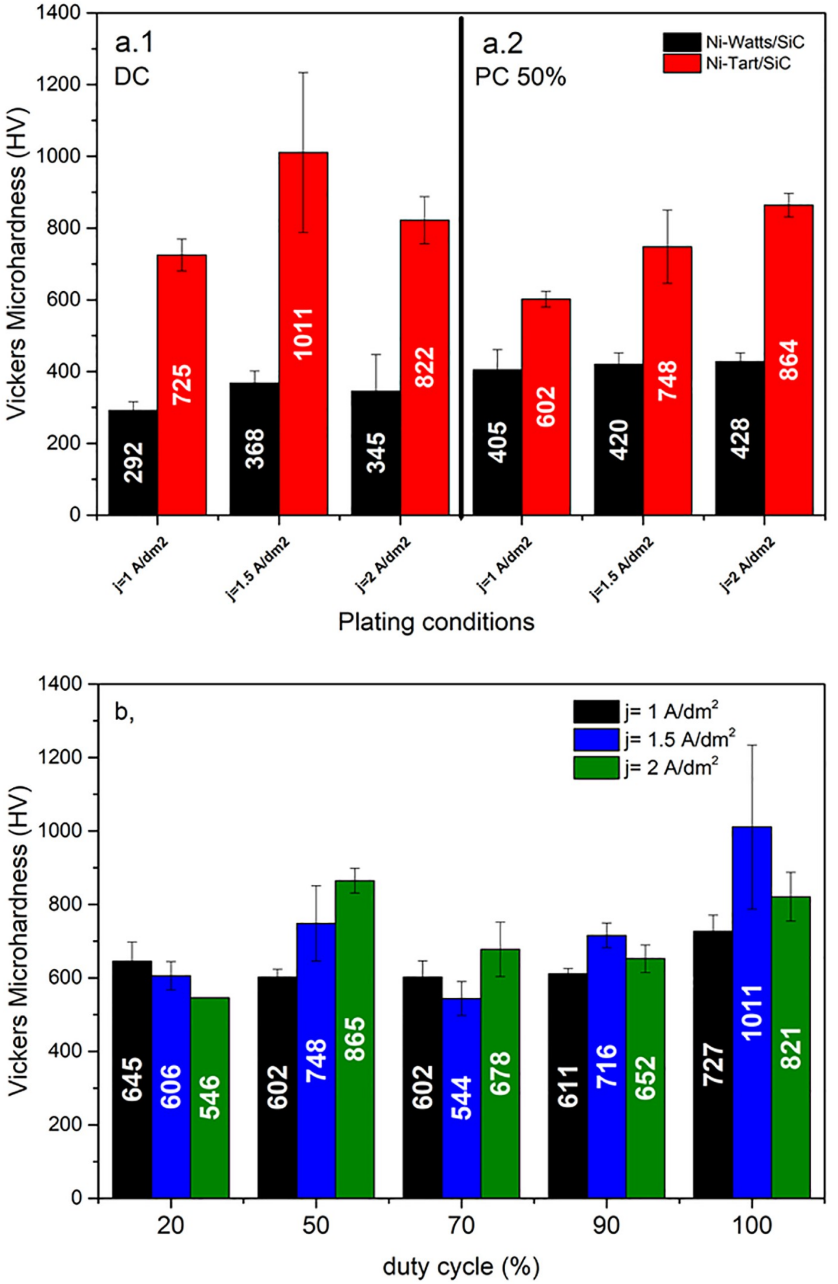

Figure 8.
Vickers microhardness of (a) Ni/SiC coatings plated from Ni-watts/SiC bath (black) and from Ni-tart/SiC bath (red). (b) Ni/SiC coatings plated from Ni-tart/SiC with PC method (d.c. 20%–100%) at j = *1.0 (black), 1.5 (blue), and 2.0 (green) A/dm*^{2}.

conditions. This remarkable result clearly outperforms the microhardness values obtained for Ni/SiC coatings produced with the industrial Ni-Watts bath.

Further investigations were carried out to evaluate the effect of PC conditions on the hardness of Ni/SiC coatings electrodeposited from the Ni–tartaric/SiC bath. Duty cycles were varied between 20% and 90% at a fixed frequency of 10 Hz, with experiments performed at current densities of 1.0, 1.5, and 2.0 A/dm^2. The resulting microhardness values are presented in **Figure 8(b)**. For reference, a d.c. of 100% corresponds to DC plating.

At a current density of 1.0 A/dm^2, relatively stable hardness values were obtained. For PC-plated samples, the values ranged narrowly between ~ 600–650 HV, increasing to 727 ± 44 HV with DC plating (100% d.c.). At j = 1.5 A/dm^2, the microhardness varied significantly with the d.c., reaching a maximum of 748 ± 102 HV at 50% d.c. under the PC plating method, which was substantially lower than the 1011 ± 223 HV achieved under DC plating. For a current density of 2.0 A/dm^2, the highest microhardness obtained was 865 ± 33 HV at 50% d.c., a value statistically comparable to that recorded for the DC-plated Ni/SiC nanocomposite coatings. No correlation was identified between hardness and decreasing d.c. or an increase in relaxation time within the cycle, as previously suggested in the study by Gyftou et al. [10]. In contrast, our results indicate that the highest microhardness values in Ni/SiC coatings can be achieved either by DC plating at j = 1.5 A/dm^2, or by PC plating at 50% d.c. with j = 2.0 A/dm^2. It should be emphasized that no average microhardness values exceeding 1,000 HV were achieved under any variation of PC plating conditions.

The Vickers microhardness values for pure Ni, as well as for Ni/Gr and Ni/WS_2 nanocomposite coatings, are presented in **Figure 9**. The coatings were deposited from Ni–tartaric acid-based electrolytes by DC plating at current densities of 1.0, 1.5, 2.0, and 5.0 A/dm^2.

The replacement of boric acid with tartaric acid resulted in an increase in microhardness values between 540 and 700 HV compared to the pure Ni coating, as shown by the black columns in **Figure 9(a)**. These values depend on the applied current density. The incorporation of Gr into the electrolyte produced Ni/Gr nanocomposite coatings with slightly higher microhardness, reaching 711 ± 132 HV at j = 1.0 A/dm^2 and 673 ± 86 HV at j = 2.0 A/dm^2, with values generally remaining between 600 and 700 HV across the investigated current densities. These values were higher than the average microhardness of Ni/Gr plated from the conventional Watts bath, reported at 500 HV [31].

A substantial increase in microhardness was observed when WS_2 NPs were introduced into the plating bath at j = 1.0 A/dm^2. The average microhardness of the Ni/WS_2 coating exceeded 1,100 ± 157 HV. Comparable high values, up to 1,280 HV, have been reported for Ni/WS_2 coatings deposited from a Ni-sulfamate bath containing boric acid [32], attributed to the uniform dispersion and high incorporation content of WS_2 nanosheets in the Ni-matrix. A slight decrease to 994 ± 174 HV was measured on Ni/WS_2 coatings plated at j = 1.5 A/dm^2 with a further decrease to 740 ± 82 HV at j = 2.0 A/dm^2. Increasing the current density to 5.0 A/dm^2 led to a slight recovery, with an average hardness of 870 ± 140 HV. Overall, the Ni/WS_2 coatings plated from Ni-tartaric acid electrolytes exhibited higher hardness values than those reported in the literature for Ni/WS_2 coatings produced under similar conditions from conventional Ni baths containing boric acid [12, 32].

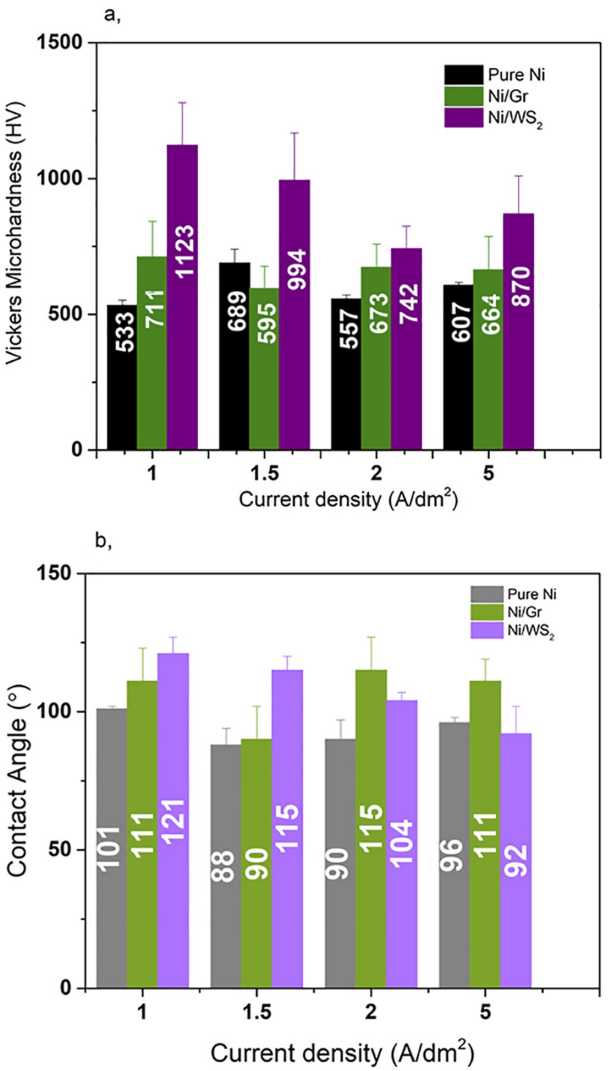

Figure 9.
(a) Vickers microhardness of pure Ni (black), Ni/G (green), and Ni/WS_2 (purple) plated from Ni-tartaric acid-based baths. (b) Water contact angle of the same coatings: pure Ni (gray), Ni/Gr (light green), and Ni/WS_2 (light purple) plated using DC method at j = 1.0, 1.5, 2.0, and 5.0 A/dm^2.

The measured water CA values of the electroplated coatings are shown in **Figure 9(b)**. For Ni/Gr and Ni/WS_2 nanocomposite coatings, the incorporation of the nanoplatelets into the Ni matrix was expected to increase surface hydrophobicity, resulting in higher CA values compared with the Ni coating [33]. As shown in **Figure 9(b)**, higher CA values were indeed obtained in the presence of Gr (green columns) or WS_2 (light purple columns) compared to the CA of pure Ni (gray columns). Specifically, the CA of the Ni/Gr coatings increased to 111° ± 12° from 101° ± 1° at j = 1.0 A/dm^2 and to 115° ± 12° from 90° ± 7° at j = 2.0 A/dm^2. It should be mentioned, though, that the influence of Gr was relatively modest, and the resulting CA values remained significantly lower than literature values of 145°–154° reported

at higher current densities (3.0–6.0 A/dm^2) [33]. In contrast, WS_2 nanosheets are known to impart hydrophobic characteristics to coatings due to their intrinsic hydrophobicity [34]. When incorporated into the Ni-matrix, WS_2 nanosheets modified the surface chemistry and enhanced the overall wettability characteristics, leading to surfaces with significantly improved hydrophobic properties.

This effect was attributed to the intrinsically low surface energy of WS_2, which promotes the formation of hydrophobic surfaces and can enhance coatings' performance in applications requiring reduced water adhesion and enhanced durability [35]. The incorporation of WS_2 nanosheets into the Ni-coatings resulted in increased hydrophobicity, as indicated by the higher CA values presented in the light purple columns in **Figure 9(b)**. The highest recorded CA was found at 121° ± 6° at j = 1.0 A/dm^2 under the DC plating method, compared to 101° ± 1° for pure Ni-coatings under the same conditions. Finally, at j = 1.5 A/dm^2 under DC, the introduction of WS_2 nanosheets led to an increase in the CA from 90° ± 7° (pure Ni) to 115° ± 8°.

These results further demonstrate the role of WS_2 in enhancing the hydrophobicity of the coatings. The combined microhardness and CA measurements confirm that 2D Gr and WS_2 nanoplatelets were successfully incorporated into the Ni matrix, forming Ni/Gr and Ni/WS_2 nanocomposite coatings. These findings are in agreement with SEM observations, which verified the incorporation of Gr and WS_2 into the Ni-matrix.

3.4.2 Pilot-scale electroplated Ni/SiC nanocomposite coatings

The same characterization methods for mechanical properties used for lab-scale coatings were applied to coatings produced at the pilot scale. Additionally, the Si-content of the coatings was determined by XRF. The average microhardness values (a) and average Si content (b) of the coatings are presented in **Figure 10**. Error margins were calculated for coatings deposited under both DC and PC methods, with both U/S_{off} and U/$S_{on/off}$ dispersion treatments. The findings were in alignment with those obtained at the lab scale. For DC-plated coatings, the average Vickers microhardness exceeded 1000 HV, indicating favorable wear resistance, a critical property for piston rod applications. Slightly lower hardness values were obtained for PC-plated samples with U/S_{off} treatment, though they remained above 900 HV (914 ± 105 HV). In contrast, when PC plating was combined with U/$S_{on/off}$ treatment, the average microhardness values decreased to 748 ± 90 HV. This reduction may be attributed to the combined effect of U/S and PC, which promotes grain growth rather than nucleation [15]. According to the Hall–Petch relationship, smaller grain sizes enhance hardness, while larger crystallites generally lead to a reduction in it [36]. This trend was consistent with the Ni/SiC coating deposited under PC and U/$S_{on/off}$, which exhibited the largest crystallite size (D_{av} = 23 nm (see **Figure 2 (a)**)) and correspondingly the lowest microhardness among the tested conditions.

The Si-content of the coatings, as measured by XRF, ranged between 2.5 and 10.5 wt%. No clear correlation was identified between Si-content and Vickers microhardness. This may be attributed to the limitations of the XRF-method, which does not provide direct information on volume fraction, particle distribution, or whether SiC is embedded, agglomerated, or exposed on the surface. A high Si-signal can also originate from surface clusters that did not reinforce the matrix effectively.

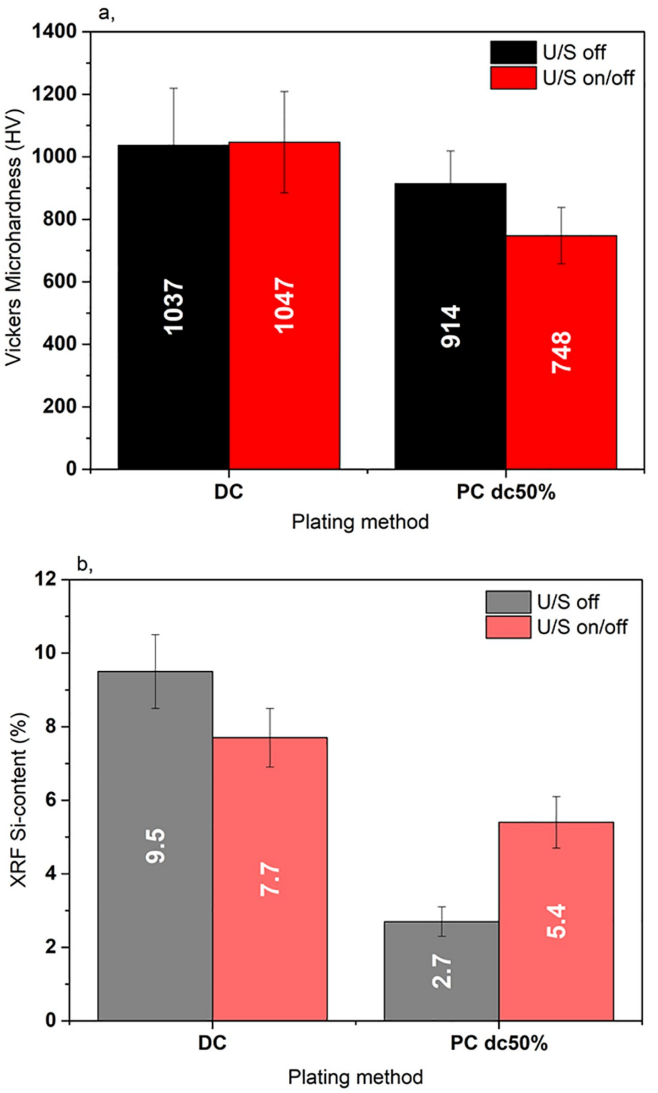

Figure 10.
(a) Average microhardness and (b) XRF result of Si-content in wt% of Ni/SiC coatings using DC or PC methods with j = *1.5 A/dm*^{2} *and U/S*$_{off}$ *(black and gray columns) and U/S*$_{on/off}$ *(red-shaded columns).*

Nevertheless, the Si-content values measured by XRF were in good agreement with those determined by EDS analysis and presented in Section 3.3.

3.5 Electrochemical studies on corrosion properties

3.5.1 Lab-scale electroplated Ni/Np nanocomposite coatings

The corresponding Tafel plots for coatings prepared at j = 1.0 A/dm^2 are shown in **Figure 11(a)**. The lowest corrosion rate (CR) of ~14 μm/year was observed for Ni/Gr (blue) and Ni/SiC (red), representing nearly a 50% reduction compared to pure Ni

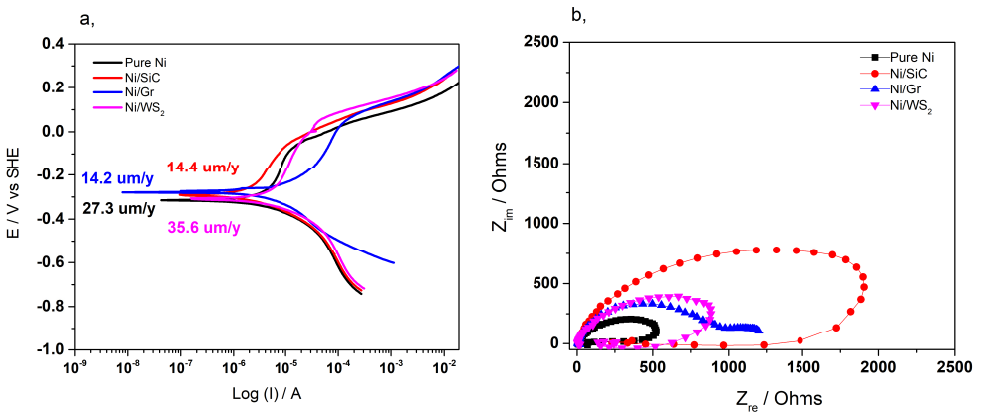

Figure 11.
(a) Tafel polarization curves and (b) Nyquist plots measured on pure Ni (black), Ni/SiC (red), Ni/Gr (blue), and Ni/WS_2 (magenta) coatings plated from Ni-tartaric acid-based baths with the plating method at j = *1.0 A/dm^2.*

(27.3 μm/year, black). In contrast, Ni/WS_2 exhibited a CR of 35.6 μm/year (magenta). These values are in agreement with literature data for coatings deposited from boric acid–based Ni baths, in which CRs of 82.2 μm/year for pure Ni, 34.8 μm/year for Ni/Gr, 16.3 μm/year for Ni/WS_2 [35], and 5.8 μm/year for Ni/SiC [37] were reported. CRs obtained from the Tafel plots for coatings deposited from Ni–tartaric acid–based baths, with and without NP incorporation under DC plating at current densities of 1.0–5.0 A/dm^2, are summarized in **Table 3**. Across this current density range, no coating exhibited a CR above 64 μm/year, which is in close agreement with values reported for Ni and Ni/NP nanocomposite coatings plated from boric acid–containing Ni baths [35, 37]. The elevated CRs observed for Ni/Gr and Ni/WS_2 in some plating conditions are most likely linked to particle-related microstructural defects. Specifically, Gr restacking may form conductive networks that promote local galvanic effects or accelerate charge transfer, while WS_2 tends to induce nodular or porous morphologies that facilitate electrolyte penetration. These findings suggest that the role of Gr can be either protective or detrimental,

	Corrosion rate (μm/year)			
***j* (A/dm^2)** **Samples**	**1.0**	**1.5**	**2.0**	**5.0**
Pure Ni	27.3	9.9	30.6	8.6
Ni/SiC	14.4	41.4	36.9	23.6
Ni/Gr	14.3	63.3	46.4	39.1
Ni/WS_2	35.6	14.4	50.5	33.4

Table 3.
Corrosion rates calculated from the I_{corr} values extracted from the Tafel polarization plots on pure Ni and Ni/Nps nanocomposite coatings plated from a Ni-tartaric acid-based bath using the DC plating method.

depending on its defect density, dispersion, and deposition parameters, whereas the effect of WS_2 on corrosion resistance is strongly morphology-dependent.

The impedance spectra of the coatings – Pure Ni, Ni/SiC, Ni/Gr, Ni/WS_2 – electrodeposited at j = 1.0 A/dm^2 are shown in **Figure 11(b)**. The smallest semicircle diameter, corresponding to the lowest charge transfer resistance (R_{ct}), was observed on the Pure Ni (black) coating, indicating more facile electron transfer and thus higher corrosion at the interface. This is consistent with an unreinforced electrodeposited Ni layer that is more active for electrolyte penetration at the electrode/electrolyte interface. The Ni/WS_2 (magenta) and Ni/Gr (blue) exhibited intermediate behavior between Ni and Ni/SiC. Regarding the Ni/WS_2 coatings, the intrinsic hydrophobicity of WS_2 likely contributed to partial blocking of diffusion pathways. However, it should be noted that partial access of the electrolyte might be enabled due to the nodular morphology of WS_2, resulting in only a moderate R_{ct} increase [12]. Similarly, the Ni/Gr coatings displayed an R_{ct} improvement compared to Pure Ni. This improved electrochemical performance can be attributed to Gr's high intrinsic conductivity, large specific surface area, and ability to form effective interfacial contact with the electrolyte [38]. A finite-length diffusion, potentially due to limited ion transport, was identified at low frequencies. This phenomenon might be attributed to structural features in the Ni/Gr, such as tortuous Gr pathways or compact electrode morphology, leading to a mixed behavior that is neither fully capacitive nor entirely diffusion-controlled [39]. The largest semicircle in diameter, corresponding to the highest R_{ct}, was exhibited for the Ni/SiC (red) coating. This indicated superior corrosion resistance compared to the other coatings, likely due to the incorporation of SiC and a more dense coating structure that hinders charge transfer [4].

3.5.2 Pilot-scale electroplated Ni/SiC nanocomposite coatings

The comparative evaluation of the Tafel polarization plots for lab-scale Ni/SiC coatings (black) and pilot-scale plated Ni/SiC (red), both deposited by the DC plating regime at j = 1.5 A/dm^2 is depicted in **Figure 12(a)**. The pilot-scale Ni/SiC

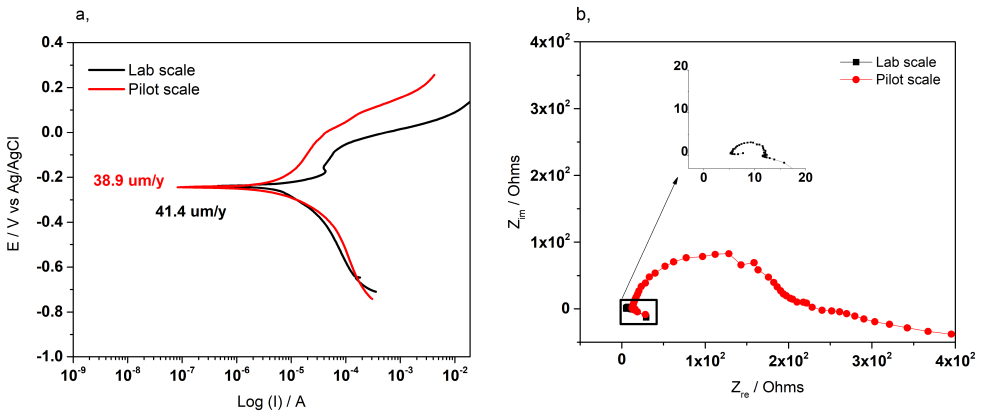

Figure 12.
(a) Tafel polarization plots and (b) Nyquist plots of Ni/SiC coatings plated at lab-scale (black) and at pilot-scale (red) using the DC plating method with U/S_{off} during plating, plated at j = 1.5 A/dm^2.

coating exhibited a slightly lower CR (38.9 μm/year) compared to the corrosion rate of the lab-scale plated sample (41.4 μm/year). This level of reproducibility indicated that Ni/SiC coatings produced from the Ni–tartaric acid bath can be reliably scaled up to pilot production. In contrast, a pronounced difference was observed in the impedance response. As shown in the Nyquist plots in **Figure 12(b)**, the pilot-scale coating (red curve) displayed a larger semicircle diameter in the high-frequency region, corresponding to a higher charge transfer resistance. This suggests enhanced resistance to electrolyte penetration at the coating's surface and indicates the potential for improved long-term corrosion protection [40].

4. Conclusions

This work demonstrated the successful implementation of tartaric acid as a REACH-compliant, environment-friendly substitute for boric acid in Watts-type Ni plating baths. Using this approach, Ni-based nanocomposite coatings were electrodeposited as a viable alternative to HC coatings, offering superior mechanical and electrochemical properties.

At the laboratory scale, tartaric acid-based electrolytes facilitated the deposition of well-defined Ni/SiC nanocomposite coatings under both DC and PC regimes. The successful incorporation and uniform distribution of SiC NPs in the Ni matrix were confirmed by XRD, SEM, and EDS. The pure Ni coatings generally exhibited microhardness values below 600 HV, whereas Ni/SiC coatings reached significantly higher values, with a maximum of 1011 ± 223 HV under DC at 1.5 A/dm^2. These results not only reach but surpass the microhardness typically associated with hard chrome coatings (i.e., ~1,000 HV), underlying the potential of Ni/SiC as a replacement for protective applications.

Investigations into Ni/2D nanocomposite coatings (Ni/Gr, Ni/WS_2) revealed a strong dependence of mechanical and surface properties on the plating parameters. Ni/WS_2 demonstrated the highest microhardness (1,123 ± 156 HV, at j = 1.0 A/dm^2), as well as the greatest hydrophobicity (CA of 121° ± 6°), highlighting WS_2 as an effective reinforcing phase in Ni-based coatings. Electrochemical studies confirmed that the use of Ni–tartaric acid baths facilitated the electrodeposition of Ni/NP coatings with improved corrosion resistance relative to pure Ni. The best performance was observed for Ni/SiC and Ni/Gr, while Ni/WS_2 showed only moderate improvement compared to pure Ni.

Pilot-scale electrodeposition on piston rods further validated the industrial feasibility of this approach. Four plating strategies were evaluated: DC and PC plating, with (U/$S_{on/off}$) and without (U/S_{off}) U/S-assistance during plating. All coatings exhibited a predominant Ni(111) crystallographic orientation. The smallest crystallites (11 nm) were achieved under DC with U/$S_{on/off}$, correlating with enhanced microstructural refinement. SEM and EDS results confirmed that SiC NPs are well dispersed across the Ni matrix. In the case of the U/$S_{on/off}$ method, a layered coating structure was produced, consisting of alternating SiC-rich and SiC-poor layers, with the latter forming during the U/S periods in the electrolyte. However, the microhardness values remained consistently high, indicating a robust reinforcing effect from the SiC NPs throughout the coating thickness. Average microhardness exceeded 1,000 HV for DC-plated coatings (1,037 ± 182 HV) and reached 1,047 ± 162 HV with DC and U/$S_{on/off}$ mode. The Si-content was determined to be around 8–12

wt% for DC-plated samples, whereas PC plating produced reduced microhardness values correlating with lower Si incorporation levels (2.5–6 wt%).

Concluding, tartaric acid was validated as a sustainable, industrially viable alternative to boric acid for electrodeposition of high-performance Ni-based nanocomposite coatings. DC plating combined with U/$S_{on/off}$-dispersion treatment proved the most effective method, achieving high microhardness and uniform NP incorporation. These findings not only provide a scalable pathway for replacing environmentally hazardous hard chrome processes but also establish a robust platform for producing advanced nanostructured coatings with superior mechanical and corrosion-resistance properties.

Acknowledgments

This research work has received funding from the European Union's Horizon Research and Innovation Program under GA No. 101058450 (MOZART).

Author details

Alexandros Zoikis Karathanasis*, Kata Berkesi, Angeliki Nikolaou, Alexios Grigoropoulos and Ioanna Deligkiozi
Creative Nano PC, Metamorfosi, Athens, Greece

*Address all correspondence to: a.karathanasis@creativenano.gr

References

[1] Bai A, Hu -C-C. Effects of electroplating variables on the composition and morphology of nickel–cobalt deposits plated through means of cyclic voltammetry. Electrochimica Acta. 2002;**47**(21):3447–3456. DOI: 10.1016/S0013-4686(02)00281-5

[2] Wang S, Ma C, Walsh FC. Alternative tribological coatings to electrodeposited hard chromium: A critical review. Transactions of the Institute of Metal Finishing. 2020;**98**(4):173–185. DOI: 10.1080/00202967.2020.1776962

[3] Di Bari GA. Electrodeposition of Nickel. In: Schlesinger M, Paunovic M, editors. Modern Electroplating Hoboken, New Jersey, USA. 1st ed. Wiley; 2010. p. 79–114. DOI: 10.1002/9780470602638.ch3

[4] Zhang H, Wang J, Chen S, Wang H, He Y, Ma C. Ni–SiC composite coatings with improved wear and corrosion resistance synthesized via ultrasonic electrodeposition. Ceramics International. 2021;**47**(7):9437–9446. DOI: 10.1016/j.ceramint.2020.12.076

[5] Wang B, et al. Deposition mechanism and corrosion resistance of Ni-Graphene composite coatings prepared by pulse electrodeposition. International Journal of Electrochemical Science. 2021;**16**(6):210636. DOI: 10.20964/2021.06.54

[6] Georgiou EP, et al. High performance accelerated tests to evaluate hard Cr replacements for hydraulic cylinders. Coatings. 2021;**11**(12):1511. DOI: 10.3390/coatings11121511

[7] Zellele DM, Yar-Mukhamedova GS, Rutkowska-Gorczyca M. A review on properties of electrodeposited nickel composite coatings: Ni-Al2O3, Ni-SiC, Ni-ZrO2, Ni-TiO2 and Ni-WC. Materials. 2024;**17**(23):5715. DOI: 10.3390/ma17235715

[8] Kan H, Meng Y, Reddy RG. Influence of particle size and surfactants on uniformity and quantity of silicon carbide particles in electrodeposited nickel-silicon carbide coatings. Journal of Central South University. 2021;**28**(6):1627–1636. DOI: 10.1007/s11771-021-4722-x

[9] Sohrabi A, Dolati A, Ghorbani M, Monfared A, Stroeve P. Nanomechanical properties of functionally graded composite coatings: Electrodeposited nickel dispersions containing silicon micro- and nanoparticles. Materials Chemistry and Physics. 2010;**121**(3):497–505. DOI: 10.1016/j.matchemphys.2010.02.014

[10] Gyftou P, Pavlatou EA, Spyrellis N. Effect of pulse electrodeposition parameters on the properties of Ni/nano-SiC composites. Applied Surface Science. 2008;**254**(18):5910–5916. DOI: 10.1016/j.apsusc.2008.03.151

[11] Liu Y, et al. Grain refinement induced friction reduction and anti-wear performances of electrodeposited graphene/Ni composites with low content reduced graphene oxide. Journal of Alloys and Compounds. 2020;**826**:154080

[12] He Y, Sun WT, Wang SC, Reed PAS, Walsh FC. An electrodeposited Ni-P-WS2 coating

with combined super-hydrophobicity and self-lubricating properties. Electrochimica Acta. 2017;**245**:872–882. DOI: 10.1016/j.electacta.2017.05.166

[13] Tudela I, Zhang Y, Pal M, Kerr I, Cobley AJ. Ultrasound-assisted electrodeposition of thin nickel-based composite coatings with lubricant particles. Surface and Coatings Technology. 2015;**276**:89–105. DOI: 10.1016/j.surfcoat.2015.06.030

[14] García-Lecina E, García-Urrutia I, Díez JA, Fornell J, Pellicer E, Sort J. Codeposition of inorganic fullerene-like WS2 nanoparticles in an electrodeposited nickel matrix under the influence of ultrasonic agitation. Electrochimica Acta. 2013;**114**:859–867. DOI: 10.1016/j.electacta.2013.04.088

[15] Pinate S, Eriksson F, Leisner P, Zanella C. Effects of SiC particles codeposition and ultrasound agitation on the electrocrystallisation of nickel-based composite coatings. Journal of Materials Science. 2021;**56**(33):18463–18476. DOI: 10.1007/s10853-021-06483-z

[16] Wachter P, Neelamegam R, Hartmann P, Schulz K-D. Nickel electroplating bath for depositing a decorative nickel coating on a substrate. Journal of Nanoscience and Nanotechnology. 2021;EP3642396B1

[17] Zoikis-Karathanasis A, Pavlatou EA, Spyrellis N. Pulse electrodeposition of Ni–P matrix composite coatings reinforced by SiC particles. Journal of Alloys and Compounds. 2010;**494**(1–2):396–403. DOI: 10.1016/j.jallcom.2010.01.057

[18] Zhang W, et al. Effects of graphene oxide and current density on structure and corrosion properties of nanocrystalline nickel coating fabricated by electrodeposition. Colloids and Surfaces A: Physicochemical and Engineering Aspects. 2022;**648**:129220

[19] Faulkner LL, Bard AJ. Electrochemical Methods and Applications. 2nd ed. New York: Wiley; 2001

[20] Pandey A, Dalal S, Dutta S, Dixit A. Structural characterization of polycrystalline thin films by X-ray diffraction techniques. Journal of Materials Science: Materials in Electronics. 2021;**32**(2):1341–1368. DOI: 10.1007/s10854-020-04998-w

[21] Péter L. Experimental methods in characterization of nanosystems. In: Scholz F, editor. Electrochemical Methods of Nanostructure Preparation, in Monographs in Electrochemistry. Cham: Springer International Publishing; 2021. p. 55–75. DOI: 10.1007/978-3-030-69117-2_3

[22] Rao H, et al. Electrodeposition of high-quality Ni/SiC composite coatings by using binary non-ionic surfactants. Molecules. 2023;**28**(8):3344. DOI: 10.3390/molecules28083344

[23] Rao H, Li W, Luo Z, Liu H, Zhu L, Chen H. Nucleation and growth mechanism of Ni/SiC composite coatings electrodeposited with micro- and nano-SiC particles. Journal of Materials Research and Technology. 2024;**30**:3079–3091. DOI: 10.1016/j.jmrt.2024.04.008

[24] Guan T, Zhang N. Recent advances in electrodeposition of Nickel-Based nanocomposites enhanced with lubricating nanoparticles.

Nanomanufacturing and Metrology. 2024;**7**(1):25. DOI: 10.1007/s41871-024-00245-6

[25] Li H, et al. Construction and anti-corrosion behavior study of silanol-modified Ni-WS2 superhydrophobic composite coating. Surface and Coatings Technology. 2022;**450**:129008

[26] Zanella C, Lekka M, Bonora PL. Effect of ultrasound vibration during electrodeposition of Ni–SiC nanocomposite coatings. Surface Engineering. 2010;**26**(7):511–518. DOI: 10.1179/174329409X438961

[27] Mbugua NS, Kang M, Zhang Y, Ndiithi NJ, Bertrand GV, Yao L. Electrochemical deposition of Ni, NiCo Alloy and NiCo–ceramic composite coatings—A critical review. Materials. 2020;**13**(16):3475. DOI: 10.3390/ma13163475

[28] Li G, et al. Investigation on microstructure and properties of the electrodeposited Ni-SiC composite coating. Coatings. 2023;**13**(4):695. DOI: 10.3390/coatings13040695

[29] Liu Y, et al. Control of the microstructure and mechanical properties of electrodeposited graphene/Ni composite. Materials Science and Engineering A. 2018;**727**:133–139

[30] Zhang JQ, Jin HM, Gao JC, Shi J, Li L. Properties of pulse plating Ni-SiC nano-composite coating. Advanced Materials Research. 2011;**291–294**: 228–232. DOI: 10.4028/www.scientific.net/AMR.291-294.228

[31] Jabbar A, et al. Electrochemical deposition of nickel graphene composite coatings: Effect of deposition temperature on its surface morphology and corrosion resistance. RSC Advances. 2017;7(49):31100–31109. DOI: 10.1039/C6RA28755G

[32] Guan T, Zhang H, Fang F, Zhang N. Synthesis of two-dimensional WS2/nickel nanocomposites via electroforming for high-performance micro/nano mould tools. Surface and Coatings Technology. 2022;**437**:128351. DOI: 10.1016/j.surfcoat.2022.128351

[33] Zhang R, Liu J, Xing X, Cui G, Li Z, Bi Z. One-step electrodeposition and fractal analysis of a novel Ni-graphene superhydrophobic coating. Colloids and Surfaces A: Physicochemical and Engineering Aspects. 2022;**654**:130128. DOI: 10.1016/j.colsurfa.2022.130128

[34] Liu J, Guo Y, Wang Z, Xing X, Cui G. Enhancement of superhydrophobicity in Ni-WS2-PTFE composite coatings via magnetic coupling electrodeposition. Surface and Coatings Technology. 2025;**497**:131731. DOI: 10.1016/j.surfcoat.2025.131731

[35] Sriraman KR, Raman SGS, Seshadri SK. Corrosion behaviour of electrodeposited nanocrystalline Ni–W and Ni–Fe–W alloys. Materials Science and Engineering A. 2007;**460-461**:39–45. DOI: 10.1016/j.msea.2007.02.055

[36] Lumley R, Morton A, Polmear I. Nanoengineering of metallic materials. In: Hannink RHJ, Hill AJ, editors. Nanostructure Control of Materials. Cambridge, UK: Woodhead Publishing Limited; 2006. p. 219–250. DOI: 10.1533/9781845691189.219

[37] Li H, et al. Influence of pulse frequency on corrosion resistance and mechanical properties of Ni-W/B4C composite coatings. Colloids and

Surfaces A: Physicochemical and Engineering Aspects. 2021;**629**:127436

[38] Szeptycka B, Gajewska-Midzialek A, Babul T. Electrodeposition and corrosion resistance of Ni-Graphene composite coatings. Journal of Materials Engineering and Performance. 2016;**25**(8):3134–3138. DOI: 10.1007/s11665-016-2009-4

[39] Azizpour A, et al. Electrochemical analysis of carbon-based supercapacitors using finite element modeling and impedance spectroscopy. Energies. 2025;**18**(6):1450. DOI: 10.3390/en18061450

[40] Cui L, et al. Research on the corrosion resistance of electrodeposited Ni-SiC composites constructed for steel storage tank application. Materials. 2024;**17**(18):4616. DOI: 10.3390/ma17184616